HHS Public Access

Author manuscript

Am J Chin Med. Author manuscript; available in PMC 2016 May 19.

Published in final edited form as:

Am J Chin Med. 2016 April ; 44(2): 321–353. doi:10.1142/S0192415X16500191.

Pyranocoumarin tissue distribution, and plasma metabolome and prostate transcriptome impacts of sub-chronic exposure to Korean *Angelica* supplement in mice

Jinhui ZHANG, PhD[1,*], **Li LI, PhD**[1,#], **Suni TANG, PhD**[1], **Yong ZHANG, MD**[1], **Maciej MARKIEWSKI, MD, PhD**[2], **Chengguo XING, PhD**[3], **Cheng JIANG, MD**[1], and **Junxuan LÜ, PhD**[1,*]

[1]Department of Biomedical Sciences, Texas Tech University Health Sciences Center School of Pharmacy, Amarillo, Texas, USA

[2]Department of Immunotherapeutics and Biotechnology, Texas Tech University Health Sciences Center School of Pharmacy, Abilene, Texas, USA

[3]Department of Medicinal Chemistry, College of Pharmacy, University of Minnesota, Minneapolis, Minnesota, USA

Abstract

Herbal products containing Korean *Angelica gigas* Nakai (AGN) root extract are marketed as dietary supplements for memory enhancement, pain killing, and female menopausal symptom relief. We have shown anti-cancer activity of AGN supplement in mouse models. To facilitate human anti-cancer translational research, we characterized the tissue distribution of AGN marker pyranocoumarin compounds decursin (D) and decursinol angelate (DA) (~50% in AGN) and their metabolite decursinol (DOH), assessed safety of sub-chronic AGN dietary exposure in mice, and explored the impacts on the plasma aqueous metabolites and prostate transcriptome. The data show that after a gavage dose, plasma contained readily detectable DOH, but little D and DA, mirroring patterns in the liver. Extra-hepatic tissues retained greater level of DA and D than liver. For sub-chronic exposures, male mice were provided *ad libitum* AIN93M-pellet diet with 0.5 and 1% AGN for 6 weeks. No adverse effect was observed on plasma biochemistry markers of liver and kidney integrity in spite of their enlargement. Histopathological examination of liver, kidney and other visceral organs did not reveal tissue abnormalities. Metabolomic assessment of plasma from the mice fed 1%-AGN diet suggested metabolic shifts of key amino acids especially methionine-cysteine cycle, purine cycle and glycolysis-citrate cycle. Prostate transcriptomic profiling identified gene signature changes of metabolisms of drugs, lipids and cellular energetics, neuro-muscular features, immunity and inflammation, and tumor suppressor/oncogene balance.

[*]Corresponding Authors: Junxuan Lü, Ph.D, Department of Biomedical Sciences, School of Pharmacy, Texas Tech University Health Sciences Center. 1300 S. Coulter St, Amarillo, TX 79106. Phone 1-806-414-9208, junxuan.lu@ttuhsc.edu. Jinhui Zhang, Ph.D, Department of Biomedical Sciences, School of Pharmacy, Texas Tech University Health Sciences Center. 1300 S. Coulter St, Amarillo, TX 79106. Phone 1-806-414-9216, jinhui.zhang@ttuhsc.edu.

[#]Current address: Center for Drug Evaluation and Research, Food and Drug Administration, Silver Spring, Maryland, USA.

Disclosure of Potential Conflicts of Interest: All authors have no personal or financial conflict of interest and have not entered into any agreement that could interfere with our access to the data on the research or on our ability to analyze the data independently, to prepare articles, and to publish them.

The safety profile was corroborated with daily *i.p.* injection of AGN extract (200 mg/kg) for 4 weeks, which resulted in much greater systemic pyranocoumarin exposure than dietary route.

Keywords

Angelica gigas Nakai; decursin; decursinol angelate; decursinol; tissue distribution; plasma metabolome; prostate transcriptome; safety assessment

Introduction

Herbal products containing Korean *Angelica gigas* Nakai (AGN) root extract are marketed as dietary supplements for pain killing, memory enhancement and female menopausal symptom relief in the United States with little rigorous human trial evidence. Of two publicized human studies, one evaluated an AGN supplement for efficacy against Alzheimer's type dementia in Korean elderly patients (Kim et al., 2003) and the other tested an AGN-containing three-herbal mixture for menopausal syndrome relief in US women (Chang et al., 2012). Accidental over-dosing and chronic use above recommended dosages of these products are of public health concern.

Pyranocoumarin isomers decursin (D) and decursinol angelate (DA) (Fig. 1A) are the major phytochemicals in the ethanol extract of AGN root. The anti-cancer, neuro-protective, pain killing and other biological activities of D and DA as well as AGN extract in cell culture and preclinical models have been documented in the past two decades and have been comprehensively reviewed (Zhang et al., 2012; Lu et al., 2015). We have recently shown chemopreventive activity of AGN extract against prostate carcinogenesis in a mouse model (Zhang et al., 2014) and that D and DA partially accounted for its efficacy (Tang et al., 2015). Although D and DA were identified by our group as novel and potent androgen receptor (AR) inhibitors in cell culture (Jiang et al., 2006; Guo et al., 2007), we and others have demonstrated that D and DA are rapidly converted to the much less potent AR inhibitor decursinol (DOH, metabolism summarized in Fig. 1B) in rodents after oral gavage, *i.p.* or intravenous injection (Lee et al., 2009; Li et al., 2012; Park et al., 2012; Li et al., 2013b). In a recently completed human pharmacokinetic (PK) study, we have shown that the PK behavior of D and DA is qualitatively the same between human and rodents (Zhang et al., 2015a), supporting the mouse as a relevant species for acquisition of crucial pyranocoumarin tissue distribution and safety data to promote human translational research consideration in terms of cancer prevention application of AGN or the pyranocoumarins. To this end, here we characterized the mouse tissue distribution patterns of D, DA and DOH in a single gavage dose-time course experiment and after repeated AGN exposures.

Only a handful of publications have included toxicological assessment of AGN extract and D or DA in rodent models (Lee et al., 2003; Kim et al., 2009; Lee et al., 2009). In two studies, the endpoints were body weight and general health (Lee et al., 2003; Lee et al., 2009). In another study (Kim et al., 2009) in which more information was acquired, the doses of 2 and 20 mg/kg D/DA in rats by oral gavage for 30 days were too low to be of toxicological relevance. A paper in Chinese language evaluated D in male and female rats using multiple toxicological endpoints for higher dosages of 125 mg/kg and 250 mg/kg

(suspended in Transcutol P) by daily intraperitoneal (*i.p.*) injection for 4 weeks (Jiang et al., 2013). There were no significant differences in the appearance, body and organ weight, food/water consumption, hematology, plasma chemistry and tissue histology between control and D-treated animals; and no apparent gender difference in these parameters. However, the rats in control group received saline instead of the actual excipients used to formulate D for *i.p.* injection. In a very recently published paper from a Korean group, the authors evaluated the genotoxicity and 13-week oral chronic toxicity of AGN hot water extract in male and female rats (Yun et al., 2015). The dose ranged from 125 to 2000 mg AGN hot water extract per kg body weight and the results indicated that AGN hot water extract was very well tolerated by rats. However, hot water was not efficient at extracting pyranocoumarins and other hydrophobic compounds from AGN. In fact, the D content in the AGN extract used in that study was 0.07% (Yun et al., 2015), more than 1000 times lower than that in the AGN ethanol extract with which our group used in PK and efficacy studies (Li et al., 2013b; Zhang et al., 2014; Tang et al., 2015).

Reliable safety information of repeated dosing of high AGN doses in animal models will inform human clinical translation beyond current use as dietary supplements. Therefore, in the present work we evaluated AGN extract by dietary administration to provide reference data for potential adverse side effects. We examined the plasma hydrophilic metabolite profiles (metabolome) and mRNA transcriptome of mouse prostate to identify potential pharmacodynamic (PD) and “toxico”-omic biomarker(s). We then confirmed the safety profile with daily *i.p.* injection of AGN extract, a route of exposure that resulted in much greater systemic phytochemical load than the alimentary route.

Material and Methods

Reagents and Chemicals

Alcoholic extract of AGN root was supplied by S.H. Kim, Kyunghee University, Republic of Korea (Tang et al., 2015). The content of D/DA of AGN extract used in this study was ~50% per HPLC-UV analysis. AGN extract was further extracted with ethyl acetate and D/DA was purified together from ethyl acetate-soluble fraction by silica chromatography. The D/DA mixture was separated on HPLC to purify D and DA as analytical standards (Li et al., 2013a). DOH was prepared by hydrolysis of D/DA as reported (Li et al., 2012). Prednisolone (internal standard (IS) for UHPLC-MS/MS), chrysin (IS for HPLC-UV), PEG400, Tween 80 and ethyl acetate were purchased from Sigma-Aldrich Co. (St. Louis, MO, USA). HPLC grade methanol and acetonitrile were from Fisher Scientific (Pittsburgh, PA, USA). B&J brand LC-MS grade water and acetonitrile were from Honeywell (Morristown, NJ, USA).

Quantitation of D, DA and DOH by HPLC-UV and UHPLC-MS/MS

Plasma samples were extracted with ethyl acetate as previously described (Li et al., 2012; Li et al., 2013b). Prostate tissue was homogenized in 20 volumes of water whereas other tissues (brain, liver, kidney, adipose, *etc.*) were homogenized in 4 volumes of water, in an ice bath. Tissue lysates and urine samples were extracted with ethyl acetate. Decursin, DA and DOH in extracts of prostate lysate were analyzed by UHPLC-MS/MS (Li et al., 2013b; Zhang et

al., 2015a). Their contents in plasma, urine and other tissue lysates were quantitated by our validated HPLC-UV method (Li et al., 2012; Li et al., 2013b) with selected samples further confirmed by UHPLC-MS/MS (Li et al., 2013b; Zhang et al., 2015a).

Preparation of diet and dosing solution

AIN-93M semi-purified diet and that diet containing 0.5% and 1% AGN extract (w/w) were prepared by Teklad Custom Research Diets (Madison, WI, USA). HPLC-UV analysis showed that D/DA content in diets was 0.24 ± 0.01% and 0.44 ± 0.004 % (mean ± SD), respectively. D/DA was not degraded after the diet was stored at 4°C for 3 months or at room temperature for 1 week. For oral gavage and *i.p.* injection, AGN extract and D/DA were administered in 0.3 mL dosing solution containing 10% ethanol, 20% PEG400, 3.3% Tween80 and 66.7% USP 5% dextrose as previously reported (Li et al., 2012; Li et al., 2013b).

Animal experiments, blood biochemistry and histopathology

The animal use was approved by the Texas Tech University Health Sciences Center Institutional Animal Care and Use Committee (IACUC). The first experiment used a single dose gavage exposure design to provide plasma and tissues to establish D, DA and DOH tissue deposition patterns over a 24-h period. Male C57BL/6 mice (6–7 weeks, purchased from The Jackson Laboratory, Bar Harbor, ME), 5 mice per group, were each given a gastric gavage of 3 mg D/DA (1.8 mg D and 1.2 mg DA) (~120 mg/kg body weight) in 0.3 mL dosing solution containing 10% ethanol, 20% PEG400, 3.3% Tween80 and 66.7% USP 5% dextrose. At indicated time points, blood was taken from anesthetized mice *via* cardiac puncture with heparin sodium as anti-coagulant to prepare plasma. Liver, kidney, lung, brain, prostate and epididymal adipose were dissected, snap frozen and stored at −80°C until analyzed for D, DA and DOH content.

In the second experiment, three groups of male C57BL/6J mice (6 weeks of age, purchased from The Jackson Laboratory, Bar Harbor, ME), 10 mice per group, were fed AIN-93M diet or that diet containing 0.5% or 1% AGN for 6 weeks. Mice were monitored daily for appearance of any signs of discomfort, and body weight and food consumption (estimated by the amount of food disappeared from the mouse feeder in each cage) were recorded twice per week. At termination of the AGN feeding experiment, mice were anesthetized in the afternoon between 1 pm and 4 pm for blood collection *via* cardiac puncture with heparin sodium as anti-coagulant to prepare plasma and sacrificed. Major visceral organs such as liver, kidney, lung, heart, and spleen were inspected, dissected, weighed, and then symmetrically cut into two parts. One part was snap frozen on dry ice and then stored in −80°C freezer for biochemical and molecular analyses. The remaining part was fixed in 10% neutral buffered formalin for histopathology. As the target organ of our cancer chemoprevention interest, the prostate was dissected and weighed and banked as above.

Plasma biochemistry panel including ALT (alanine aminotransferase), AST (aspartate transaminase), ALP (alkaline phosphatase), creatinine and BUN (blood urea nitrogen) was measured at Texas A & M University Veterinary Medical Diagnostic Laboratory Amarillo. H&E-stained sections of major visceral organs were examined in a blinded fashion to the

treatment status by study pathologists Maciej Markiewski, MD, PhD (co-author, Texas Tech University Health Sciences Center) or James Trybus, DVM (Texas A&M University Veterinary Medical Diagnostic Laboratory Amarillo).

Profiling of endogenous aqueous metabolites in mouse plasma

The protocol published by Yuan *et al* (Yuan et al., 2012) was adopted to profile endogenous metabolites in mouse plasma. This protocol used hydrophilic interaction liquid chromatography with positive/negative ion switching to monitor near 300 MRM transitions from a single LC-MS/MS acquisition with a 5 milliseconds dwell time. Plasma samples from mice fed 1%-AGN diet and control AIN-93M diet were mixed with 4 volumes of pre-cooled (−80 °C) methanol. After 8 h at −80 °C, the mixtures were centrifuged at 14,000g for 10 minutes and the supernatants were subjected to analysis on an UHPLC system (Nexera, Shimadzu) combined with a hybrid triple quadruple linear ion trap mass spectrometer (QTRAP 5500, AB Sciex). Chromatographic separation was performed on an XBridge BEH Amide Column (100mm×4.6mm, 3.5μm, Waters). The column oven temperature was kept at 40°C. Each sample was analyzed by four UHPLC-MS/MS runs with the injection volume of 10 and 1μL. Homoscedastic, two-tailed Student's t-test was used to determine whether the peak area (indication of abundance) of each metabolite was significantly different between mice fed control or 1% AGN diet.

Microarray and real-time qRT-PCR analysis of prostate tissue

Total RNAs were extracted from mouse prostate (3 mice per group; whose plasma was analyzed for hydrophilic endogenous metabolites) using RNeasy Mini kit (QIAGEN). mRNA expression profiles of prostate from mice fed control diet and 1% AGN diet were analyzed using Illumina Mouse Ref-8 BeadChip expression array. Equal amount of RNAs from three mice in each group were pooled together. RNA labeling and hybridization was performed at the BioMedical Genomics Center of the University of Minnesota according to protocols specified by the manufacturers (Zhang et al., 2014). Real-time PCR was performed for individual samples as previously described using the Fast Start Universal SYBR Master with ROX (Roche) with an ABI 7300 Real Time PCR System (Applied Biosystems) (Zhang et al., 2014). β-actin was used as a normalization control. Primers specific for each genes are listed in Table 1. Statistical significance of signal detection was determined by homoscedastic, two-tailed Student's t-test. Web based bioinformatics tool IMPaLA (Integrated Molecular Pathway Level Analysis) (Kamburov et al., 2011) version 7 were employed for pathway over-representation and enrichment analysis.

Safety evaluation of parenteral AGN exposure

Since early PK studies by us and others have shown attainment of greater plasma pyranocoumarin C_{max} and AUC by *i.p.* injection than gavage (Li et al., 2012), we carried out the third experiment aiming to further escalate the systemic AGN exposure load by daily *i.p.* injection of increasing dosages of 100, 200 or 300 mg/kg (in 0.3 mL), six days per week for 4 weeks. Four groups of CD-1 mice, 12 mice per group (6 each sex), 8–10 weeks of age (purchased from Charles River Laboratories, Wilmington, MA), were fed AIN-93M control diet and received vehicle or the different AGN dosages. Concentrations of AGN dosing solution were adjusted based on body weight weekly. Blood was taken at 3 h after the last

AGN administration. Major visceral organs were collected as in the second experiment and examined histologically by our study pathologists. Plasma biochemistry panel was carried out the same as in the second experiment. A different strain of mice was chosen because of their genetic similarity to SCID mice used in our concurrent xenograft anti-cancer efficacy studies.

Statistical analyses

The mean and SD (in some cases medium and range) were presented for each experimental group. Differences among groups were analyzed by one way ANOVA using PRISM statistical analysis software, when the data distribution conformed to normality and homogeneity requirements (GraphPad Software, Inc., La Jolla, CA). For comparison involving only two groups, Student's t-test was used. Significant differences were calculated at $P<0.05$.

Results

Tissue D, DA, DOH deposition patterns after a single gavage dose

Published plasma PK studies in mice and rats by us and others have strongly supported extensive first-pass liver conversion of D and DA to DOH (Park et al., 2012; Li et al., 2013a; Li et al., 2013b) (as summarized in Fig 1B). To address weather extra-hepatic organs such as prostate, the target tissue of our interest for cancer chemoprevention, might retain and metabolize D and DA differently from the liver, we performed a single dose experiment with D/DA mixture to relate plasma PK profiles with tissue deposition patterns.

To rule out possible artifacts of tissue sample processing, we tested the stability of D and DA in freshly prepared tissue lysates at both 37°C and 4°C (ice bed). At 37°C, about 50% of D/DA was converted to DOH in the liver, kidney and lung lysates, whereas ~20% D/DA were converted to DOH in adipose lysate after 1 hour. At 4°C, only ~10% D/DA were converted to DOH in liver lysate, whereas almost no conversion in the lysates of other tissues after 1 hour (Data not shown). These findings suggest a possibility of some D and DA conversion to DOH in extra-hepatic tissues, but liver possesses the most significant metabolic flux given the first-pass nature of intestine/mesentery absorption and the liver mass in relation to other visceral organs.

The UHPLC-MS/MS method allowed us to quantitate D and DA separately (Li et al., 2013b; Zhang et al., 2015a) and their respective contents in different organs over time are shown in Fig. 2. The T_{max} for D, DA and DOH in plasma and all analyzed organs was at 1 hour (earliest sampled point). C_{max} of DOH in plasma (39.8 μM) (Fig. 2A) and all analyzed organs were in comparable magnitude (Fig. 2B, liver: 47.8 μmol/kg; Fig. 2C, kidney: 50.4 μmol/kg; Fig. 2D, prostate: 46.4 μmol/kg; Fig. 2E, lung: 31.6 μmol/kg; Fig. 2F, brain: 23.3 μmol/kg; Fig. 2G, adipose: 28.5 μmol/kg). The peak contents of DA in all the analyzed organs were greater than in plasma such that DA C_{max} in liver, kidney, lung, brain, prostate and adipose was 2.95, 5.51, 3.13, 1.78, 14.80 and 7.26 μmol/kg, respectively, vs. C_{max} of plasma DA of 0.76 μM. For D, the C_{max} in plasma and liver, kidney, lung, brain, prostate and adipose was 0.38 μM, and 0.38, 0.42, 0, 1.00, 4.90 and 1.75 μmol/kg, respectively, lower

than respective DA values. Prostate and epididymal adipose had the greatest amount of peak DA and D among the analyzed organs. Overall, the tissue distribution kinetics of D, DA and DOH after a single dose suggested pharmacological relevance of DA, and to a lesser extent, of D retained in the extra-hepatic target organs, in addition to DOH.

Safety parameters of male mice fed AGN-diets for 6 weeks

In AGN-diet feeding experiment for 6 weeks with male C57BL/6J mice, none of the mice died before termination and their appearance was normal. No bleeding and infection or inflammation of visceral organs was visible at necropsy. In the first week, mice consumed less 1%-AGN diet than control or 0.5%-AGN diet (Fig. 3B), presumably due to the strong odor of AGN and consequently, lost body weight (Fig. 3A). After the adaptive period, there was no difference in the food intake and mean body weight among mice of all three groups. Normalized liver weight (Fig. 3C) in 0.5%- and 1%-AGN groups was each 32% greater than the control group ($p<0.05$). Normalized kidney weight (Fig. 3D) in 0.5%- and 1%-AGN group was 9% and 12% greater than control group ($p<0.05$). Normalized weights of heart, spleen, lung and thymus were not different among three groups (Data not shown).

Histopathological examination of H&E-stained sections by study pathologists did not identify any major lesions in the liver and kidney or other organs of the AGN-fed mice. Consistent with histology, plasma assays of liver, integrity ALP, AST, ALT (Fig 3F–H) and kidney function, BUN and creatinine (Data not shown) indicated that they were not adversely impaired in the AGN-fed mice. The normalized prostate weight was significantly less in the mice fed 1%-AGN diet (Fig. 3E, 27% less than control group) but was not affected in the mice fed 0.5%-AGN diet. Therefore, as major metabolic and detoxification organs, liver and kidney in the AGN-fed mice underwent adaptive responses in their sizes to metabolize the ingested AGN phytochemicals including D and DA.

Plasma and tissue D, DA and DOH after sub-chronic dietary exposure

Terminal-bleed (6–9 h since light cycle started in morning) plasma levels of DOH in mice fed 0.5%- and 1%-AGN diet were 0.99 ± 0.11 and 2.44 ± 0.52 μM (mean ± SE, n=5), respectively. Parent compounds D and DA were below limit of detection by HPLC-UV, except only in one mouse from the 1%-AGN diet group (0.67 μM D/DA, quantitated together). The tissue contents of DOH and D/DA were 41.1 and 0 μmol/kg in liver; 14.43 and 1.20 μmol/kg in kidney; 3.33 and 1.6 μmol/kg in lung; 2.97 and 1.77 μmol/kg in brain; and 12.8 and 3.00 μmol/kg in prostate (n=3). Both HPLC-UV and UHPLC-MS/MS chromatograms showed that DA was more abundant than D in all organ lysates. Together, the data indicated that even though circulating level of D/DA was extremely low; there could be considerable D/DA retained in most extra-hepatic organs after 6 weeks of dietary exposure. The lack of detectable hepatic D/DA was consistent with liver first-pass metabolism as the major pathway to convert D/DA to DOH by human cytochrome 2C19 and 3A4 isoforms and additional D conversion to DOH by carboxyesterase-2 (summarized in Fig. 1B) (Park et al., 2012; Zhang et al., 2015b).

Effect of consumption of AGN diet on plasma endogenous metabolites

We profiled the endogenous metabolites in the plasma of male C57BL6 mice (3 from control group and 3 from 1%-AGN diet group). Each mouse plasma extract was analyzed by duplicate UHPLC-MS/MS runs with the injection volume of 10 and 1μL each because the abundance of each endogenous metabolite varied over a wide range. This approach enabled us to quantitate the majority of plasma endogenous metabolites within valid dynamic range.

Table 2 listed plasma aqueous metabolites that significantly differed between control mice and 1%-AGN fed mice (t-test, $p<0.05$, $n=3$). Nine metabolites were found increased in the plasma of AGN fed mice by 20% or higher. For oxidized glutathione disulfide (GSSG) and S-adenosyl-L-homocysteine, data acquired in both positive and negative ion modes were almost the same. Six of these metabolites were related to Methionine-Cysteine Cycle important for many metabolic reactions including DNA methylation (homocysteine, S-adenosyl-L-homocysteine, dimethylglycine, S-adenosyl-L-methionine) or Cysteine products (oxidized glutathione GSSG; taurine). Two metabolites were related to glucose metabolism: D-gluconate is a linearized oxidation product of glucose; 2,3-diphosphoglyceric acid is generated from phosphoglycerate mutase (rich in erythrocytes)-catalyzed diversion of glycolytic intermediate 1-phosphoglycerate. Increased FAD could be a reflection of decreased citrate cycle flux at the succinate-fumarate reaction that requires and drives FAD $\rightarrow FADH_2$ redox.

Eleven metabolites were decreased in the plasma of AGN fed mice by 20 % or more in descending order (Table 2). The citrate-isocitrate and leucine-isoleucine isomer pairs were quantitated together since the chromatographic condition used was not able to achieve baseline separation of these respective isomers. Decreased lactate and citrate-isocitrate would be consistent with decreased glycolytic and citrate cycle flux. The majority of plasma metabolite reductions observed in the AGN-fed mice involved decreased key amino acids (lysine, leucine-isoleucine, tyrosine, threonine, 1-methyl-histidine and ornithine, which is a key urea cycle intermediate of urea release from arginine).

Although the p values for aminoadipic acid, a lysine metabolite, was greater than 0.05 between the means of the two groups, we included it due to potential clinical relevance (Jung et al., 2013) which was reported significantly increased in prostate cancer tissues from radical prostatectomy compared to matched normal adjacent tissue. In addition, Kaplan-Meier curves for biochemical recurrence-free time after surgery showed that higher cancer tissue aminoadipic level segregated with poor prognosis ($p=0.025$). In that paper, the levels of arginine, leucine/isoleucine, lysine, ornithine, threonine and tyrosine were also significantly higher in prostate cancer. In our samples, the plasma level of these amino acids and metabolites was significantly decreased in the AGN-fed mice (Table 2). In addition, levels of adenine, the precursor of adenosine and aminoimidazole carboxamide ribonucleotide, an analog of adenosine were lowered. suggesting a shrunken adenosine pool. This might be a consequence of increased use of adenosine in the Methionine-Cysteine Cycle (e.g., increased S-adenosyl-homocysteine; S-adenosyl-L-methionine). Therefore, the data suggest AGN consumption resulted in shifts of systemic sulfur-amino acids and products (increase) and key branch-chain and essential amino acids and glycolysis and

citrate cycle flux (decrease), suggesting patterns conducive to drug metabolism and cancer risk reduction.

Effect of consumption of AGN diet on gene expression signatures in the mouse prostate

Given that we had shown in the androgen-dependent human LNCaP prostate cancer cell model D or DA dose-dependently suppressed AR-target gene PSA expression at mRNA and protein levels with IC_{50} of 1 ~ 1.3 μmol/L (Jiang et al., 2006; Guo et al., 2007) and the observed accumulation of DA, and to much less extent of D, in mouse prostate, we analyzed the effect of AGN feeding on AR-target genes in mouse prostate using real time qRT-PCR. Compared to the control mice, those consuming 1%-AGN diet significantly decreased their prostate mRNA abundance of AR target genes *Pbsn* (probasin), *Nkx3.1* and *Msmb* (β-microseminoprotein, PSP94) (Fig. 4A, n=3) (mice do not have *KLK3*/PSA gene). As an androgen-responsive organ, the normalized prostate weight of the 1% AGN diet-fed mice was reduced by 27% compared to that of control mice (Fig. 3D, n=10).

We recently reported that AGN gavage treatment significantly inhibited the growth of AR-independent neuroendocrine carcinomas (NE-Ca) in TRAMP (transgenic adenocarcinoma of mouse prostate) mice (Zhang et al., 2014). The efficacy was associated with the inhibition of angiogenesis (FGF axis and VEGF axis), epithelial-mesenchymal transition (EMT)/metastasis and inflammation pathways. To test whether AGN modulated the expression of these genes in the non-carcinogenic prostate, we surveyed some of them by qRT-PCR. As can be seen from Fig. 4A, AGN-diet consumption suppressed the expression of *Fgfbp3* (fibroblast growth factor binding protein 3), *Tgfbr2* (transforming growth factor b receptor II), and *Col1a2* (collagen type I alpha 2); and increased the expression of *Actc1* (Actin alpha cardiac muscle 1), which is known to be lower in human prostate cancer than in normal prostate tissue.

We further explored the effect of 1%-AGN feeding on the prostate global gene expression signatures by microarray using the same RNA samples. The AGN diet did not affect the expression of two housekeeping genes, *Actb* (beta-actin) and *Gapdh* (glyceraldehyde-3-phosphate dehydrogenase) (Table 3). The expression of 133 annotated genes was increased by more than 60% (AGN/basal ratio >1.6) (Table 3). On the other hand, the mRNA expression of 37 genes was suppressed by 1%-AGN diet for more than 40% (AGN/basal ratio <0.6) (Table 4). They were tabulated into major function categories based on literature, however, a few were inferred from sequence/structural similarity with homologs or gene family members. As detection validation, the microarray-detected changes for *Cyp2b10, Foxa1* (less than 40% cut off threshold), *CCND1, Defb42* and *LCN2* were confirmed by qRT-PCR with reasonable concordance of modulation directions (Fig 4B).

AGN-induced genes (Table 3)—Thirteen genes were related to Phase I (cytochrome p450 isoforms) or Phase II drug metabolism, including 3 glutathione S-transferases (known tumor suppressors in prostate). Twenty five genes were related to Inflammation and Immune responses, e.g., *Saa3* (serum amyloid A 3); *Lcn2* (lipocalin 2, aka NGAL, neutrophil gelatinase-associated lipocalin, involved in innate immunity by sequestrating iron to limit bacterial growth) and several *Defn* (defensin) genes. A large group of genes were involved in

Lipid/PPAR metabolism or energy metabolism, e.g., several apolipoproteins such as *Apoa1-3* (apolipoprotein A-1-III); *Mup1-3* (major urinary proteins 1–3), which are usually secreted by liver and excreted in urine that act as male sexual pheromones; and 3 creatine kinases.

A prominent group of genes were related to Muscle features, e.g., *Atp2a1* (ATPase, Ca++ transporting, cardiac muscle, fast twitch 1); *Myl1* (myosin, light polypeptide 1); *Mylp* (myosin light chain, phosphorylatable, fast skeletal muscle); *Tnni2* (troponin I, skeletal, fast 2); *Tnnc2* (troponin C2, fast). Six genes were related to Neurogenesis and Neuroprotection, e.g., *Ttr* (transthyretin); *Pvalb* (parvalbumin). Considering the prostate glandular secretory functions are controlled "on demand" during ejaculatory process, the increased neuro-muscular gene expression signatures might indicate enrichment of such cell types such as neuron-endocrine and smooth muscles as a consequence of decreased prostate mass (secretory epithelium) in the AGN-fed mice.

Another large group of genes have potential tumor suppressor functions, e.g., proteases inhibitors such as Serpins, Kazal type serine peptidase inhibitors, and *Ambp* (alpha-1-microglobulin/bikunin); *Wfdc10* (WAP four-disulfide core domain 10). Additional gene categories included Solute Transporters (e.g., aquaporins; transferrin), Redox and Vascular health, and even 5 oncogene-like genes, e.g., *Mia1* (melanoma inhibitory activity 1).

Interestingly, corresponding to plasma metabolite increases of S-adenosyl-L-methionine, taurine and 2,3-diphosphoglyceric acid (Table 2), the prostate mRNA transcript level of *Mat1a* (methionine adenosyltransferase I, alpha) (Methionine-Cysteine metabolism), *Cdo1* (cysteine dioxygenase 1, cytosolic) (Taurine production) and *Pgam2* (phosphoglycerate mutase 2) (rich in erythrocytes for synthesis of 2,3-diphosphoglycerate that is an allosteric enhancer of hemoglobin oxygenation) was higher in AGN-fed mice by 1.8 to 2.5 fold (Table 3).

AGN-suppressed genes (Table 4)—Out of 37 genes down-regulated by 40% or greater, 20 genes were Oncogene-like or pro-carcinogenic (Table 4). Many, if not all, genes have been reported to be higher in cancerous tissues and/or to promote tumor growth, progression and invasion. *Nupr1* (nuclear protein 1) was one of the most substantially down-regulated genes in prostate by AGN feeding (decreased by 71%). It is a small, highly basic and loosely folded protein inducible by cellular stresses. Recent studies in breast, lung, colon and other cancer models suggest *Nupr1* might be a new drug-targetable protein for preventing cancer progression and metastasis (Chowdhury et al., 2009; Cano et al., 2011). Clinical data also indicated that the mRNA expression of *Nupr1* was increased in lymphoma, brain and prostate cancer (www.oncomine.org). Three genes related to prostate function were suppressed: *Abpb* (androgen binding protein beta) (decreased by 73%); *Adi1* (acireductone dioxygenase 1); *Svs3b* (seminal vesicle secretory protein 3B), perhaps linked to the decreased prostate weight (e.g., secretory epithelium).

The observed decrease of prostate mRNA levels in the AGN-fed mice of *Cox8b* (cytochrome c oxidase, subunit VIIIb) (brown adipose tissue BAT mitochondrial thermogenesis), *Gpr83* (G protein-coupled receptor 83) (thermogenesis) and *Ucp1*

(uncoupling protein 1) (mitochondria proton carrier, BAT thermogenesis) could also be in line with decreased plasma metabolites of the citrate cycle activity (Table 2).

Taken together, both targeted detection and global profiling of the prostate gene expression changes suggested AGN consumption shifted gene signatures toward cancer risk modification by stimulating “tumor suppressor” genes and decreasing “oncogene-like” genes, in addition to gene signature changes that suggest improvements of drug metabolism and detoxification; inflammatory and immune responses; lipid metabolism, neuro-muscular health. These other potential health promoting functions of AGN, especially neuroprorection, are consistent with its multi-faceted bioactivities including memory enhancement and pain killing (Zhang et al., 2012; Lu et al., 2015).

Safety assessment of AGN by *i.p.* injection for 4 weeks in male and female mice

In the daily *i.p.* bolus exposure model, no lethality was observed in any of the dose groups. The body weight of the male mice at termination showed suppressed growth of 5–11% (Table 5). In contrast to diet feeding, *i.p.* AGN treatment did not significantly increase the normalized weight of liver over the dose range, and even decreased the normalized weight of kidney by 9.7–13% (Table 5). The normalized prostate weight, and that of lung, heart, thymus, spleen were not significantly affected (Table 5). Plasma biochemistry assays showed that ALP, AST, ALT and creatinine were not statistically different among 4 groups whereas plasma BUN was significantly lower in the AGN-treated mice (Table 5).

The body weight of female CD-1 mice was not significantly affected by AGN treatment through *i.p.* route (Table 6). AGN treatment increased normalized liver weight (6.2–15%), and dose-dependently decreased normalized weight of spleen (up to 28%) and thymus (up to 35%), but did not significantly affect normalized weight of heart, lung and kidney (Table 6). Plasma levels of ALT, AST, ALP, BUN and creatinine were not significantly affected by AGN treatment (Table 6).

At necropsy, we occasionally observed in the abdominal cavity adhesion among liver, intestine and abdominal wall as well as the edge of liver distended in some of the mice treated with the highest AGN dose of 300 mg/kg. These were likely caused by the accumulation of AGN components of poor solubility or their interaction with excipients for *i.p.* injection into the peritoneal cavity. Other than the organ adhesion noted at 300 mg/kg, we were not able to identify visible abnormalities such as infection and hemorrhage. Histopathological examination of liver, kidney and spleen by the study pathologists did not detect any major lesions from any AGN dose groups. Therefore, we estimated a No Observable Adverse Effect Level (NOAEL) of 200 mg/kg by daily *i.p.* injection in the mice.

Plasma and tissue pyranocoumarin contents after repeated *i.p.* exposures

We euthanized mice at 3 hours after they received the last *i.p.* injection of AGN extract. At this time point, concentration for D/DA or DOH in mice was after their respective peak C_{max} (Lee et al., 2009) (see also Fig. 2 oral PK). DOH concentration in terminal-bleed plasma ranged from 4.80 to 76.5 μM and D/DA concentration varied from 0 (below detectable limit) to 4.63 μM (n=4~6 per dose group), respectively. These ranges confirmed much greater systemic pyranocoumarin exposure than from the dietary feeding. DOH content in liver,

lung, kidney and brain was lower than its plasma level, whereas D/DA contents in those organs were similar to their plasma levels (Data not shown). In all organs analyzed, DA was more abundant than D.

In urine collected directly from the bladder of several AGN-injected mice at necropsy, HPLC-UV analysis showed that DOH level was much higher than that in plasma, ranging from 117 to 603 μM, yet, D/DA could not be detected in any AGN dose groups (n=4~6 per dose group). There was no obvious gender difference with respect to the above parameters between male and female mice. We observed similar urine/plasma disparity patterns in C57BL/6J mice receiving AGN extract by oral gavage. The bladder urine and kidney DOH data indicate kidney clearance for elimination of circulating DOH (summarized in Fig. 1B).

Discussion

Although we and other groups had reported the plasma PK patterns and parameters of D, DA and metabolite DOH in mice and rats, comprehensive information on the organ/tissue distribution of these compounds is very limited. To provide data for inference of possible human tissue deposition, in the current work, we used a single dose time course to profile the parent compounds and metabolite in extra-hepatic organs in the mice (Fig. 2) and analyzed them after repeated AGN exposures. In spite of extensive first-pass liver metabolism of D and DA to DOH, minor amount of DA was detected in the extra hepatic organs, suggesting enrichment by some tissues especially in prostate and adipose. Hydrophobicity of D and DA might offer an explanation for their accumulation in adipose. Incubation test of D and DA with different mouse tissue lysates confirmed liver with the most metabolizing activity and suggested the possibility of some D and DA conversion to DOH in extra-hepatic tissues. Since we showed that fresh human whole blood or fresh plasma lacked conversion activity (Zhang et al., 2015a), a tissue's ability to retain D and DA will likely be a function of the balance between influx from/efflux to blood and the tissue activity of cytochrome p450 (Cyp) isoforms and carboxyesterases (schematically summarized in Fig. 1B). Indeed, we have demonstrated that blocking Cyp activities with an orally administered general inhibitor was able to increase prostate retention of D and DA by 2 orders of magnitude (Zhang et al., 2015b). Analyses of urine collected from bladder of *i.p.*-treated mice showed high concentration of DOH and no D or DA. The absence of D and DA in urine was the same as we observed in human subjects (Zhang et al., 2015a), affirming renal clearance as an important route for DOH elimination. Based on the similar plasma PK behavior between human and rodents (Zhang et al., 2015a), the organ/tissue pyranocoumarin distribution profiles in the mice will likely be informative for extrapolation to humans.

In sub-chronic dietary exposure study for 6 weeks, 1% AGN diet induced metabolic adaptation changes in the mice to "detoxify" the phytochemical load as reflected in the increased liver and kidney weight without evidence of a compromise in their functional integrities (Figure 3). Regarding metabolomics profiling, we observed increases of plasma metabolites related to methionine-cysteine cycle and metabolism (Table 2), suggesting a major impact of AGN dietary consumption on metabolism of these sulfur-amino acids and likely single-carbon metabolism such as DNA methylation and drug conjugations mediated through their metabolites, e.g., glutathionylation and sulfation. We also observed in the

current work a significant reduction of non-sulfur key amino acids in the AGN fed mice (Table 2). Interestingly, these amino acids were reported to be elevated in prostate cancer vs. matched prostate tissue (Table 2). We also have profiled the endogenous aqueous metabolites in the TRAMP tumors vs. normal prostates from wild type littermates obtained from NCI mouse model bio-repository (Kelly-Spratt et al., 2008) (C57BL/6 background, n=3 for each group, data to be published elsewhere) and observed the tissue levels of adenine as well as the following amino acids, 1-methyl-histidine, leucine/isoleucine, ornithine, threonine and tyrosine were substantially increased in TRAMP tumors. Since these metabolites are essential amino acids or building blocks for biosynthesis, metabolic changes are likely in place in the tumor-bearing mice to supply them. Consequently, interventions like AGN feeding that decreased these metabolites would likely attenuate critical metabolic fluxes to decrease oncogenic risk.

The organ site origin(s) of the plasma metabolome changes are presently not known. Because of the observed changes of liver and kidney weight (Fig. 3), they would be prime suspects. Microarray profiling of the mRNA changes, even though in prostate, revealed that both Phase I and Phase II enzymes were among prominent genes upregulated by dietary AGN consumption (Table 3). It would be reasonable to extrapolate that these gene categories might be affected in the liver and/or kidney as well. We plan in the future to study the gene signature and metabolome changes in these and other organs to address such issues.

Since we used normal “non-carcinogenic” mice to evaluate the plasma metabolite profiles and global gene expression signatures in the prostate of the treated mice, the data could inform potential systemic health benefits and toxicity and possible risk modification for primary cancer prevention in human. With respect to carcinogenesis risk modification, some prostate genes modulated by AGN feeding countered the directions of their changes associated with TRAMP carcinogenesis reported by our group and others. In the stimulated genes, a major group was related to tumor suppressor functions (Table 3) including several families of protease inhibitors that constrict cancer cell motility and invasion, and Phase II drug metabolism GST genes, whose loss or inactivation contributes to the known etiology of human prostate cancer. Although prominently known for lipid metabolism and cardiovascular health, many apolipoproteins are involved in cancer metabolism and behavior. The prostate lipid metabolism modifying activity of AGN consumption in our study could be linked to cancer risk reduction. For example, Zamanian-Daryoush and coworkers investigated the anti-cancer effect of *ApoA1*, (apolipoprotein A1) (Zamanian-Daryoush et al., 2013) using both genetic and pharmacological approaches. ApoA1 potently suppressed tumor growth and metastasis in multiple animal tumor models, including the aggressive B16F10L murine malignant melanoma model. *In vitro* experiments ruled out direct suppressing effects of ApoA1 on cancer cells. Further studies revealed that both innate and adaptive arms of immunity contributed to the *in vivo* anti-cancer effect of ApoA1. In a human prospective study of more than 7500 French subjects, baseline plasma ApoA1 level inversely associated with overall and breast cancer risk through 14-year follow-up (His et al., 2014). Recently, higher baseline serum ApoA1 level was also associated with favorable prognosis in metastatic nasopharyngeal carcinoma (Jiang et al., 2014) and advanced non-small cell lung cancer (Cheng et al., 2015). Although higher serum level of ApoA2 was also reported to be associated with prolonged overall survival in patients with metastatic renal

cell cancer (Vermaat et al., 2010), only subcutaneous injection of ApoA1, not ApoA2, could regress established B16F10L-luciferase melanoma tumors and metastasis in ApoA1 knockout mice (Zamanian-Daryoush et al., 2013). Bioinformatic analysis indicated that lipid metabolism changes are also cross-related to PPARα signaling (e.g., *ApoA2, ApoC3, ApoA1, CYP8B1*) pathways. For the Muscle signature, many, including *Tpm2, Myl1, Tnni2* and *Tnnc2*, were down-regulated during prostate carcinogenesis and therefore could also be "tumor suppressors". A particular notable feature for these genes was that AGN gavage in the TRAMP model induced their expression in NE-Ca (Zhang et al., 2014), which is not of epithelial origin and AR-independent (Wang et al., 2011). Consistent with immune benefit that we have reported in TRAMP NE-Ca from mice treated with AGN (Zhang et al., 2014), a number of defensins (*Defb2*, *Defb11, Defb42*, *Defb43*) involved in innate immunity were up-regulated by AGN feeding in the prostate. Defensins are small bactericidal peptides through disrupting microbial membrane integrity. *In vitro* and clinical studies suggested their potential tumor suppressing activities. Future studies will determine the cell origins within prostate of the gene expression changes, many very dramatically. As the mice had been exposed to AGN feeding for 6 weeks, changes in cell types such as increase in muscle or immune cells and/or gene expression changes within a given cell type could all in theory be possible. Acute exposure time course will further help to delineate temporal sequence of gene and cellular changes to infer on cause-effect relationships.

For the suppressed genes, more than half of them were related to Oncogene-like functions (Table 4). A number of suppressed genes beside *Nupr1* also merit some elaboration. The protein level of brown fat-specific *Ucp 1* (uncoupling protein 1) increases with disease progression from normal tissue, primary cancer to bone metastases (Zhau et al., 2011). *Alah3a1* (Aldehyde dehydrogenase 3A1) was reported to correlate with the progression of prostate cancer in human, and *in vitro* and animal studies confirmed a robust up-regulation of *Aldh3a1* in human DU145-derived cancer stem cells (Yan et al., 2014). *Foxa1* (detected by qRT-PCR, Fig. 4A) modulates steroid hormone transactivation and is frequently overexpressed in metastatic castration-resistant prostate cancer (mCRPC) (Danila et al., 2014), likely by facilitating AR binding at genomic regions not normally occupied by AR (Robinson et al., 2014). It is interesting to note that a number of suppressed genes including *Abpb* (androgen binding protein beta) and *Azgp1* (alpha-zinc-2-glycoprotein1) were found upregulated by AGN in the TRAMP NE-Ca (Zhang et al., 2014) (Table 4). Whether such contrasting patterns of regulation by AGN exposure reflect differences in cell origins (e.g., neuroendocrine NE-Ca vs. mostly epithelium in normal prostate) of the gene expression changes will be of future research interest.

Our safety evaluation of AGN in mice through dietary route support no observed adverse effect level (NOAEL) of 1% in diet with respect to plasma chemistry and histopathology, corresponding to intake of 1200 mg (~ 600 mg D/DA) per kg body weight (calculated based on 3 g diet intake per day for a mouse weighing 25 g) (Fig. 3). By allometric scaling (Sharma and McNeill, 2009), the mouse NOAEL intake estimated here approximated a human equivalent dose of 100 mg AGN dietary supplement per kg body weight (~ 50 mg D/DA per kg)). Current recommended human dose for AGN dietary supplement is 800 mg per day for adult (~11 mg per kg) (Zhang et al., 2015a). The NOAEL information will therefore be a useful starting point for designing future human studies of AGN for cancer

prevention or therapeutic indications. The safety of AGN dietary exposure was corroborated with daily *i.p.* injections for 4 weeks. Measurement of the plasma and tissue contents of DOH and D/DA confirmed the parenteral route resulted in much greater systemic AGN phytochemical loads than alimentary exposure. Since 300 mg/kg dose resulted in occasional visceral organ adhesions, we estimated a NOAEL of 200 mg/kg (~100 mg/kg D/DA by i.p.) in the mice (Table 5). This would be in line with the reported safe dose of 250 mg D/kg in the rats (Jiang et al., 2013). By allometric extrapolation, a human NOAEL of 17 mg AGN/kg is estimated for *i.p.* injection exposure route (~8 mg D/DA per kg).

In conclusion, prostate and other tissue pyranocoumarin distribution data from the current work revealed small amount of parent compounds accumulated in extra-hepatic organs along with DOH as both the dominant circulating and tissue accumulated pyranocoumarin. Our safety study with sub-chronic dietary AGN exposure in mice revealed no adverse effects on liver or kidney integrity with 1% AGN diet (allometric human equivalent dose ~100 mg AGN per kg body weight), in spite of an increase of liver and kidney weight that was likely attributable to metabolic adaptation to metabolize the phytochemical load. Overall, plasma metabolomic profiling suggested metabolic shifts of key amino acids especially methionine-cysteine cycle, purine cycle and glycolysis-citrate cycle. Prostate transcriptomic microarray identified gene signature changes of metabolisms of drugs, lipids and cellular energetics, neuro-muscular features, immunity and inflammation, and tumor suppressor/oncogene balance.

Acknowledgments

This work was supported by NIH National Center for Complementary and Integrative Health grant AT007395 (J. L. C.X.), and Texas Tech University Health Sciences Center Preliminary Data Grant (J. Z.). The authors thank Dr. James Trybus, DVM (Texas A&M Veterinary Medical Diagnostic Laboratory Amarillo Laboratory) for evaluation of tissue specimens for histopathology and Wayne Chee, Pharm. D. and Mr. Debasish Basak for technical assistance.

References

Cano CE, Hamidi T, Sandi MJ, Iovanna JL. Nupr1: the Swiss-knife of cancer. J Cell Physiol. 2011; 226:1439–1443. [PubMed: 20658514]

Chang A, Kwak BY, Yi K, Kim JS. The effect of herbal extract (EstroG-100) on pre-, peri- and post-menopausal women: a randomized double-blind, placebo-controlled study. Phytotherapy research: PTR. 2012; 26:510–516. [PubMed: 21887807]

Cheng T, Dai X, Zhou DL, Lv Y, Miao LY. Correlation of apolipoprotein A-I kinetics with survival and response to first-line platinum-based chemotherapy in advanced non-small cell lung cancer. Med Oncol. 2015; 32:407. [PubMed: 25465061]

Chowdhury UR, Samant RS, Fodstad O, Shevde LA. Emerging role of nuclear protein 1 (NUPR1) in cancer biology. Cancer Metastasis Rev. 2009; 28:225–232. [PubMed: 19153668]

Danila DC, Anand A, Schultz N, Heller G, Wan M, Sung CC, Dai C, Khanin R, Fleisher M, Lilja H, et al. Analytic and clinical validation of a prostate cancer-enhanced messenger RNA detection assay in whole blood as a prognostic biomarker for survival. Eur Urol. 2014; 65:1191–1197. [PubMed: 23954088]

Guo J, Jiang C, Wang Z, Lee HJ, Hu H, Malewicz B, Lee JH, Baek NI, Jeong JH, Kim DK, et al. A novel class of pyranocoumarin anti-androgen receptor signaling compounds. Molecular cancer therapeutics. 2007; 6:907–917. [PubMed: 17363485]

His M, Zelek L, Deschasaux M, Pouchieu C, Kesse-Guyot E, Hercberg S, Galan P, Latino-Martel P, Blacher J, Touvier M. Prospective associations between serum biomarkers of lipid metabolism and overall, breast and prostate cancer risk. Eur J Epidemiol. 2014; 29:119–132. [PubMed: 24519551]

Jiang, C-z; Feng, J-m; Zhang, J-f; Han, I.; Choung, S. Decursin Safety from Root of Angelica gigas in Rats. Journal of Northeast Agricultural University (English Edition). 2013; 20:46–51.

Jiang C, Lee HJ, Li GX, Guo JM, Malewicz B, Zhao Y, Lee EO, Lee JH, Kim MS, Kim SH, et al. Potent antiandrogen and androgen receptor activities of an Angelica gigas-containing herbal formulation: Identification of decursin as a novel and active compound with implications for prevention and treatment of prostate cancer. Cancer Research. 2006; 66:453–463. [PubMed: 16397261]

Jiang R, Yang ZH, Luo DH, Guo L, Sun R, Chen QY, Huang PY, Qiu F, Zou X, Cao KJ, et al. Elevated apolipoprotein A-I levels are associated with favorable prognosis in metastatic nasopharyngeal carcinoma. Med Oncol. 2014; 31:80. [PubMed: 25023050]

Jung K, Reszka R, Kamlage B, Bethan B, Stephan C, Lein M, Kristiansen G. Tissue metabolite profiling identifies differentiating and prognostic biomarkers for prostate carcinoma. Int J Cancer. 2013; 133:2914–2924. [PubMed: 23737455]

Kamburov A, Cavill R, Ebbels TM, Herwig R, Keun HC. Integrated pathway-level analysis of transcriptomics and metabolomics data with IMPaLA. Bioinformatics. 2011; 27:2917–2918. [PubMed: 21893519]

Kelly-Spratt KS, Kasarda AE, Igra M, Kemp CJ. A mouse model repository for cancer biomarker discovery. J Proteome Res. 2008; 7:3613–3618. [PubMed: 18624399]

Kim JH, Koh SK, Koh HJ, Kwon YA, Kim SH, Kim JG, Kim TE, Park JW, Seo MY, Song YR. A three month placebo-controlled clinical trial of INM 176 in the old aged subjects with memory impairment. Journal of Korean Neuropsychiatric Association. 2003; 42:254–262.

Kim KM, Lee YJ, Hong YG, Kang JS. Oral Acute and Subacute Toxicity Studies of Decursin and Decursinol Angelate of Angelica gigas Nakai. Molecular & Cellular Toxicology. 2009; 5:153–159.

Lee HJ, Lee EO, Lee JH, Lee KS, Kim KH, Kim SH, Lu J. In vivo anti-cancer activity of Korean Angelica gigas and its major pyranocoumarin decursin. Am J Chin Med. 2009; 37:127–142. [PubMed: 19222117]

Lee S, Lee YS, Jung SH, Shin KH, Kim BK, Kang SS. Anti-tumor activities of decursinol angelate and decursin from Angelica gigas. Archives of Pharmacal Research. 2003; 26:727–730. [PubMed: 14560921]

Li L, Zhang J, Shaik AA, Zhang Y, Wang L, Xing C, Kim SH, Lu J. Quantitative Determination of Decursin, Decursinol Angelate, and Decursinol in Mouse Plasma and Tumor Tissue Using Liquid-Liquid Extraction and HPLC. Planta Medica. 2012; 78:252–259. [PubMed: 22116603]

Li L, Zhang J, Xing C, Kim SH, Jiang C, Lu J. In Vitro Metabolism of Pyranocoumarin Isomers Decursin and Decursinol Angelate by Liver Microsomes from Man and Rodents. Planta medica. 2013a

Li L, Zhang J, Xing C, Kim SH, Lu J. Single Oral Dose Pharmacokinetics of Decursin, Decursinol Angelate, and Decursinol in Rats. Planta Medica. 2013b; 79:275–280. [PubMed: 23364885]

Lu, J.; Zhang, J.; Li, L.; Jiang, C.; Xing, C. Current Pharmacology Reports. In: Kong, ANT., editor. Cancer Chemoprevention with Korean Angelica: Active Compounds, Pharmacokinetics, and Human Translational Considerations. Springer; 2015.

Park HS, Kim B, Oh JH, Kim YC, Lee YJ. First-pass Metabolism of Decursin, a Bioactive Compound of Angelica gigas, in Rats. Planta Medica. 2012; 78:909–913. [PubMed: 22573368]

Robinson JL, Hickey TE, Warren AY, Vowler SL, Carroll T, Lamb AD, Papoutsoglou N, Neal DE, Tilley WD, Carroll JS. Elevated levels of FOXA1 facilitate androgen receptor chromatin binding resulting in a CRPC-like phenotype. Oncogene. 2014; 33:5666–5674. [PubMed: 24292680]

Sharma V, McNeill JH. To scale or not to scale: the principles of dose extrapolation. British journal of pharmacology. 2009; 157:907–921. [PubMed: 19508398]

Tang S, Zhang J, Wu W, Jiang P, Puppala M, Zhang Y, Xing C, Kim S-H, Jiang C, Lü J. Chemopreventive effects of Korean Angelica vs. its major pyranocoumarins on two lineages of transgenic adenocarcinoma of mouse prostate carcinogenesis. Cancer Prevention Research. 2015; 8:835–844. [PubMed: 26116406]

Vermaat JS, van der Tweel I, Mehra N, Sleijfer S, Haanen JB, Roodhart JM, Engwegen JY, Korse CM, Langenberg MH, Kruit W, et al. Two-protein signature of novel serological markers apolipoprotein-A2 and serum amyloid alpha predicts prognosis in patients with metastatic renal cell cancer and improves the currently used prognostic survival models. Ann Oncol. 2010; 21:1472–1481. [PubMed: 20022911]

Wang L, Zhang J, Zhang Y, Nkhata K, Quealy E, Liao JD, Cleary MP, Lu J. Lobe-specific lineages of carcinogenesis in the transgenic adenocarcinoma of mouse prostate and their responses to chemopreventive selenium. Prostate. 2011; 71:1429–1440. [PubMed: 21360561]

Yan J, De Melo J, Cutz JC, Aziz T, Tang D. Aldehyde dehydrogenase 3A1 associates with prostate tumorigenesis. Br J Cancer. 2014; 110:2593–2603. [PubMed: 24762960]

Yuan M, Breitkopf SB, Yang X, Asara JM. A positive/negative ion-switching, targeted mass spectrometry-based metabolomics platform for bodily fluids, cells, and fresh and fixed tissue. Nature protocols. 2012; 7:872–881. [PubMed: 22498707]

Yun JW, Che JH, Kwon E, Kim YS, Kim SH, You JR, Kim WH, Kim HH, Kang BC. Safety evaluation of Angelica gigas: genotoxicity and 13-weeks oral subchronic toxicity in rats. Regul Toxicol Pharmacol. 2015

Zamanian-Daryoush M, Lindner D, Tallant TC, Wang Z, Buffa J, Klipfell E, Parker Y, Hatala D, Parsons-Wingerter P, Rayman P, et al. The cardioprotective protein apolipoprotein A1 promotes potent anti-tumorigenic effects. J Biol Chem. 2013; 288:21237–21252. [PubMed: 23720750]

Zhang J, Li L, Hale TW, Chee W, Xing C, Jiang C, Lu J. Single oral dose pharmacokinetics of decursin and decursinol angelate in healthy adult men and women. PLoS One. 2015a; 10:e0114992. [PubMed: 25695490]

Zhang J, Li L, Jiang C, Xing C, Kim SH, Lu J. Anti-cancer and Other Bioactivities of Korean Angelica gigas Nakai (AGN) and Its Major Pyranocoumarin Compounds. Anti-cancer agents in medicinal chemistry. 2012; 12:1239–1254. [PubMed: 22583405]

Zhang J, Li L, Tang S, Hale TW, Xing C, Jiang C, Lu J. Cytochrome P450 isoforms in the Metabolism of Decursin and Decursinol Angelate from Korean Angelica. Am J Chin Med. 2015b; 43:1211–1230. [PubMed: 26394652]

Zhang J, Wang L, Zhang Y, Li L, Tang S, Xing C, Kim SH, Jiang C, Lu J. Chemopreventive effect of Korean Angelica root extract on TRAMP carcinogenesis and integrative “omic” profiling of affected neuroendocrine carcinomas. Mol Carcinog. 201410.1002/mc.22230

Zhau HE, He H, Wang CY, Zayzafoon M, Morrissey C, Vessella RL, Marshall FF, Chung LW, Wang R. Human prostate cancer harbors the stem cell properties of bone marrow mesenchymal stem cells. Clin Cancer Res. 2011; 17:2159–2169. [PubMed: 21355075]

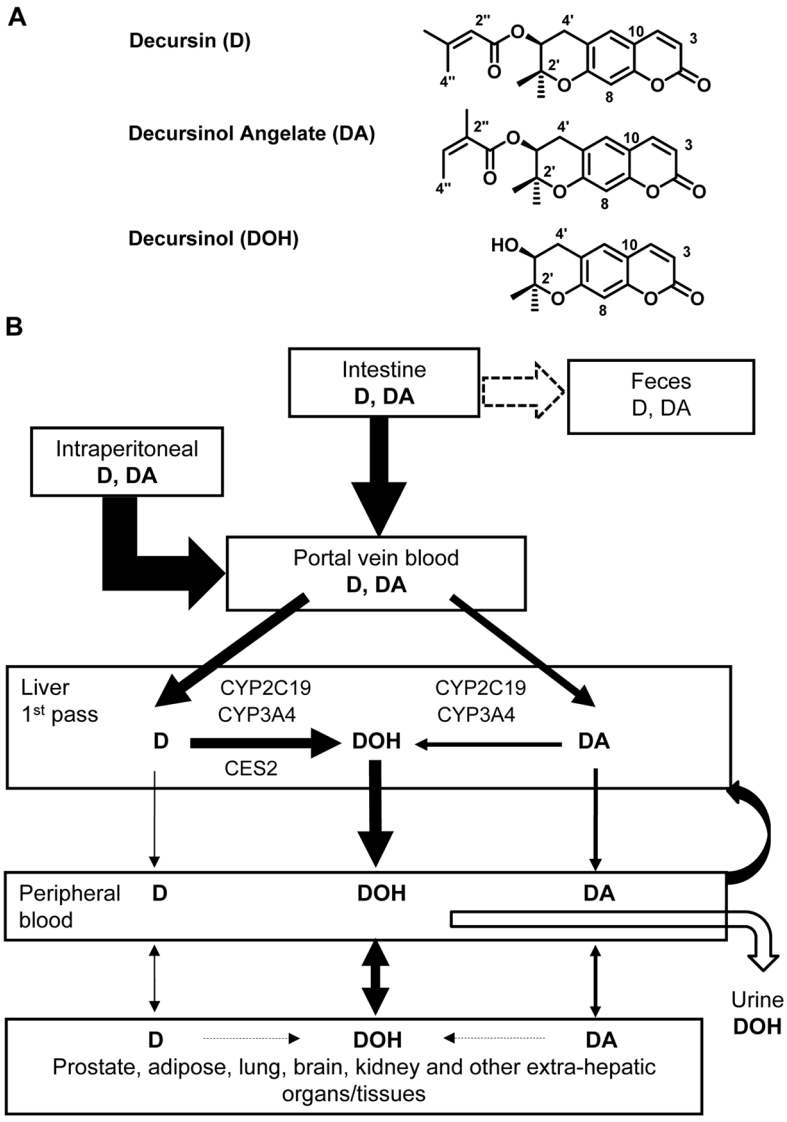

Figure 1.

Chemical structure (Panel A) of decursin (D), decursinol angelate (DA) and decursinol (DOH), and schematic integration of current knowledge (Panel B) of D and DA metabolism based on rodent data, including the current work, and human studies *in vitro* and *in vivo*. Cyp, cytochrome p450; CES, carboxyesterase.

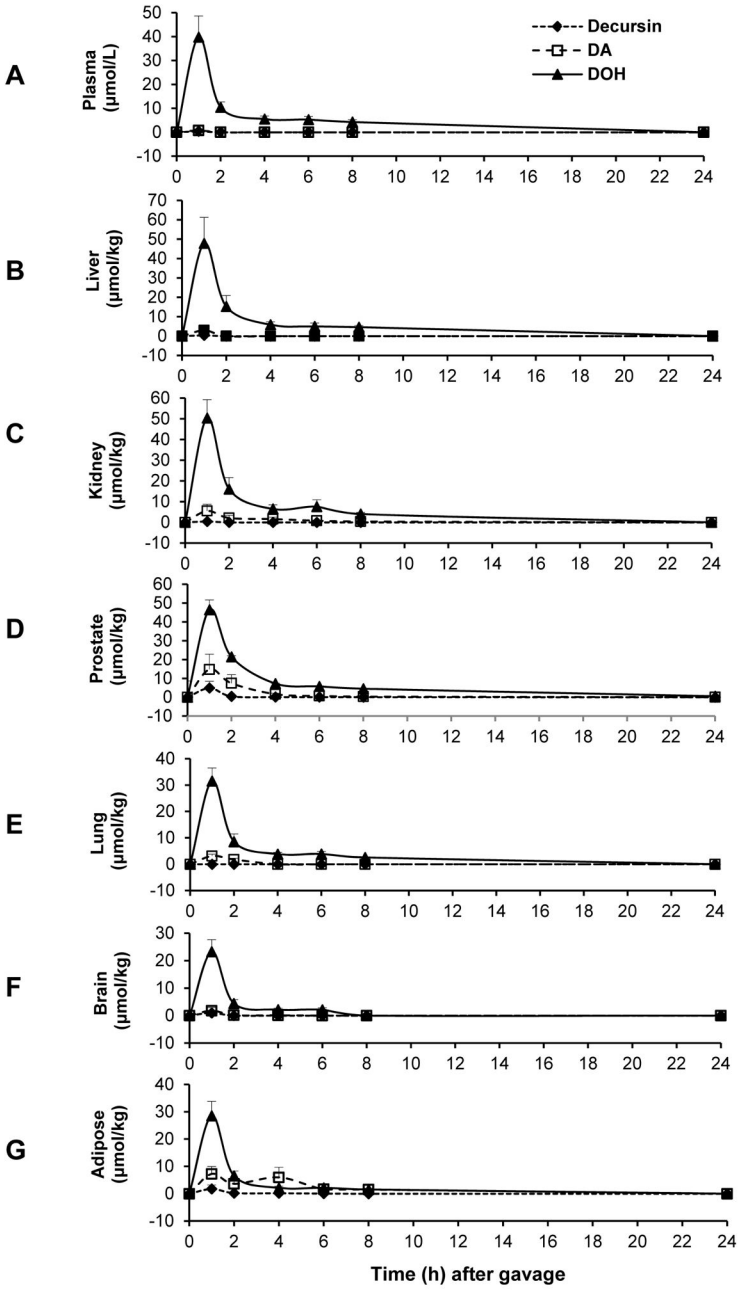

Figure 2.

Plasma and tissue profiles of D, DA and DOH after a single gavage dose of D/DA mixture (150 mg/kg) in male C57BL/6 mice. N=5 mice. Panels: A, plasma; B, liver; C, kidney; D, prostate; E, lung; F, brain; G, adipose.

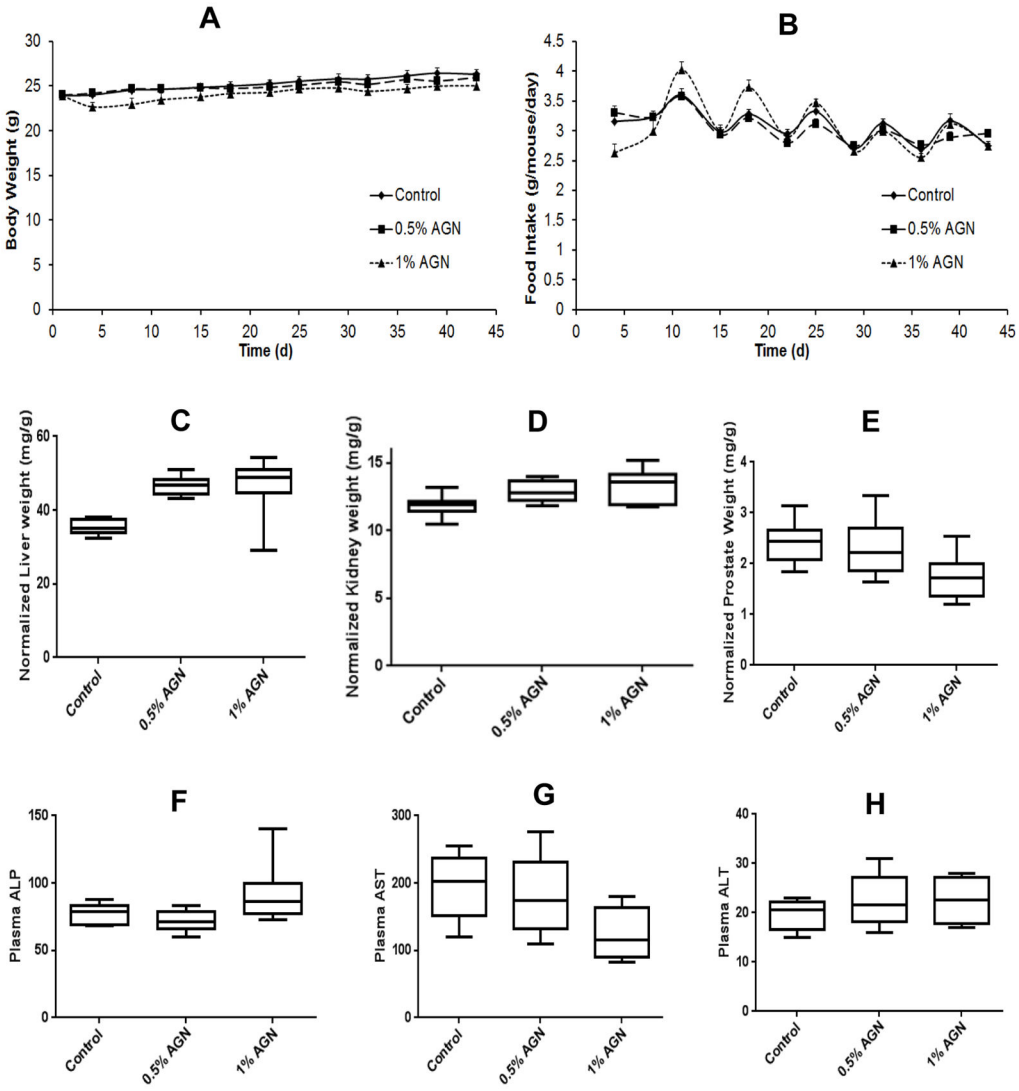

Figure 3.

Effects of feeding AGN-containing diets to male C57BL/6 mice for 6 weeks on growth, select organ weight and liver integrity markers. Body weight (A) and food intake (B) as function of feeding duration; Normalized weight of liver (C), kidney (D) and prostate (E) to body weight; Plasma ALP (F), AST (G) and ALT (H) levels as liver integrity biomarkers. N=10 mice per group.

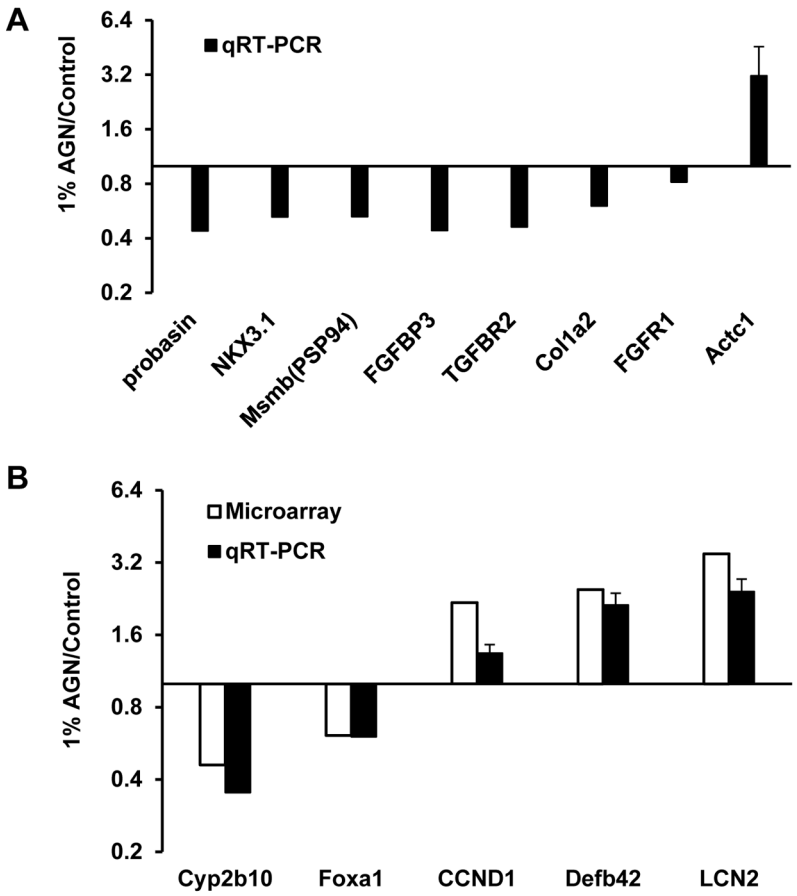

Figure 4.

Effect of 1% AGN diet on the expression of selected genes in the prostate of male C57BL/6 mice. (A) AR-regulated genes, and invasion and metastasis-associated genes detected with qRT-PCR; (B) select genes modulated by AGN detected by microarray and verified by qRT-PCR.

Table 1

Primers for qRT-PCR detection of AGN-modulated genes.

Gene Symbol	Sequence ID	Forward primer (5′-3′)	Reverse Primer (5′-3′)
β-actin	NM_007393.3	CCTAAGGCCAACCGTGAAAA	GAGGCATACAGGGACAGCACA
FGFBP3	NM_028263.1	GGGTAGGTGCTGAGAAGCAG	CCATTTTGGAATCCCGACTA
TGFBR2	NM_009371.3	CCAGAACCCACGACAAAAGT	CACCCTGCTTTGGAGACAAT
FGFR1	NM_010206.3	ACCAAGAAGAGCGACTTCCA	AACCAGGAGAACCCCAGAGT
Col1a2	NM_007743.2	CTCCCCAAAATGTTTGCAGT	GCGAATGTTCATGGGTTTCT
Actc1	NM_009608.3	TCTCTTCCAGCCCTCTTTCA	ATGGTGGTGCCTCCAGATAG
Foxa1	NM_008259.3	ACAGGGTTGGATGGTTGTGT	TGTTGCTGACAGGGACAGAG
Cyp2b10	NM_009999.4	CCAAATCTCCAGGGCTCCAAGGC	TGCGGACTTGGGCTATTGGGAGG
LCN2	NM_008491.1	TGCCACTCCATCTTTCCTGTT	GGGAGTGCTGGCCAAATAAG
CCND1	NM_007631.2	GCGTACCCTGACACCAATCT	ATCTCCTTCTGCACGCACTT
Defb42	NM_001034910.3	CATCCTGGTGACATCATTGC	GCAATCCATACCCACCCTAA
MSMB	NM_020597.3	CCAACGCTACTAGGCCTTTGA	GCCCACACGAAGCACATTTAC
Nkx3.1	NM_010921.3	ACTGAACCCGAGTCTGATGCAC	TACAGGTAGGGGTAGTAGGGATAGC
Probasin	NM_017471.2	ATCATCCTCCTGCTCACACTGCATG	ACAGTTGTCCGTGTCCATGATACGC

Am J Chin Med. Author manuscript; available in PMC 2016 May 19.

Table 2

UHPLC-MS/MS profiled plasma hydrophilic metabolites of male C57BL/6 mice fed 1% AGN diet.

Plasma Aqueous Metabolite	Mean plasma Ratio	p-value	Reported human PCa/prostate	Metabolic Function
	AGN/Control, n=3	t-test	median ratio (95% CI)	pathways
Increased in AGN fed mice				
Glutathione disulfide GSSG (positive mode)	2.34	0.009	0.96 (0.77–1.07)	Cysteine product, Redox
Glutathione disulfide GSSG (negative mode)	2.00	0.030		
Taurine	1.44	0.028	0.87 (0.78–0.99)	Cysteine product
Homocysteine	2.27	0.037		Methionine-Cysteine Cycle
S-Adenosyl-L-homocysteine (positive mode)	2.08	0.003		Methionine-Cysteine Cycle
S-Adenosyl-L-homocysteine (negative mode)	1.76	0.037		
Dimethylglycine	1.63	0.004		Methionine-Cysteine Cycle
S-Adenosyl-L-methionine	1.21	0.006	1.30 (1.20–1.62)	Methionine-Cysteine Cycle
2,3-Diphosphoglyceric acid (Hb oxygenation)	2.04	0.035		Glucose metabolism, diversion from glycolysis
D-Gluconate	1.78	0.032		Glucose oxidation product, diversion from glycolysis
Flavin adenine dinucleotide (FAD)	1.38	0.028		Citric acid cycle, Redox
Decreased in AGN fed mice				
Lysine	0.58	0.010	1.30 (1.19–1.44)	Amino acid, ketogenic
Leucine-isoleucine	0.65	0.043	1.29 (1.18–1.36)	Amino acid, ketogenic
Tyrosine	0.44	0.052	1.27 (1.15–1.48)	Amino acid
Threonine	0.59	0.038	1.26 (1.17–1.39)	Amino acid
1-Methyl-Histidine	0.64	0.028		Amino acid
Ornithine	0.62	0.030	1.42 (1.22–1.63)	Amino acid Arginine catabolism, Urea cycle
Aminoadipic acid	0.57	*0.083*	1.40 (1.13–1.63)	Amino acid Lysine metabolism
Adenine	0.46	*0.066*	1.15 (1.10–1.26)	Adenosine substrate, Purine cycle
Aminoimidazole carboxamide ribonucleotide	0.68	0.023		Adenosine analog, Purine cycle
Citrate-isocitrate	0.70	0.016		Citric acid cycle
Lactate	0.72	0.050	1.06 (0.99–1.10)	Glucose metabolism, glycolysis product

Am J Chin Med. Author manuscript; available in PMC 2016 May 19.

Table 3

Prostate transcriptomic signatures up-regulated by 1% AGN feeding in male C57BL/6 mice.
Genes in mouse prostate up-regulated by AGN diet feeding for 6 weeks

	Up-regulated in AGN fed mice >60% (Bold font >2 fold)			**AGN-regulated**
Gene Symbol	**Definition**	**AGN/Control**	**Functional category**	**in NE-Ca**
				Zhang MolCar2014
Actb	actin, beta	0.97	House keeping gene	
Gapdh	glyceraldehyde-3-phosphate dehydrogenase	1.00	House keeping gene	
Cyp4a12a	**cytochrome P450, family 4, subfamily a, polypeptide 12a**	**3.13**	**Drug metabolism, Phase I**	
Cyp4a14	cytochrome P450, family 4, subfamily a, polypeptide 14	1.61	Drug metabolism, Phase I	
Cyp2a5	**cytochrome P450, family 2, subfamily a, polypeptide 5**	**2.50**	**Drug metabolism, Phase I**	
Cyp2c37	cytochrome P450, family 2. subfamily c, polypeptide 37	1.83	Drug metabolism, Phase I	
Cyp2d9	cytochrome P450, family 2, subfamily d, polypeptide 9	1.89	Drug metabolism, Phase I	
Cyp2e1	cytochrome P450, family 2, subfamily e, polypeptide 1	1.65	Drug metabolism, Phase I	
Cyp3a11	cytochrome P450, family 3, subfamily a, polypeptide 11	1.60	Drug metabolism, Phase I	
Cyp8b1	cytochrome P450, family 8, subfamily b, polypeptide 1	1.67	Drug metabolism, Phase I	
Gsta3	glutathione S-transferase, alpha 3	1.77	Drug metabolism, Phase II, loss in PCa	
Gstm5	glutathione S-transferase, mu 5	1.62	Drug metabolism, Phase II, lost in PCa	
Mgst1	glutathione S-transferase 1, microsomal	1.93	Drug metabolism, Phase II, loss in PCa	
Sult1a1	sulfotransferase family 1A, phenol-preferring, member 1	1.70	Drug metabolism, Phase II	
Ugt2b36	UDP glucuronosyltransferase 2 family, polypeptide B36	1.92	Drug metabolism, Phase II	
Saa3	**serum amyloid A 3**	**5.19**	**Inflammation, adiposity**	
Kng1	**kininogen 1**	**3.09**	**Inflammation, coagulation**	Dn88
Ahsg	**alpha-2-HS-glycoprotein (fetuin-A)**	**2.07**	**Inflammation, inhibitory**	
Alox5ap	**arachidonate 5-lipoxygenase activating protein**	**2.04**	**Inflammation**	
Crygc	crystallin, gamma C	1.69	Inflammation, inhibitory	
Hpgd	hydroxyprostaglandin dehydrogenase 15 (NAD)	1.78	Inflammation, inhibitory	
Hpx	**hemopexin**	**2.14**	**Inflammation, heme chelator, inhibitory**	
Ifit3	interferon-induced protein with tetratricopeptide repeats 3	1.88	Inflammation	
Sgk1	serum/glucocorticoid regulated kinase 1	1.61	Inflammation	

	Up-regulated in AGN fed mice >60% (Bold font >2 fold)			AGN-regulated
Gene Symbol	Definition	AGN/Control	Functional category	in NE-Ca
				Zhang MolCar2014
Lcn2	**lipocalin 2**	**3.48**	**Immunity, innate, inflammation**	
Arg1	arginase 1, liver	1.65	Immunity, infection	
C3	complement component 3	1.64	Immunity	
Cd52	**CD52 antigen**	**2.13**	**Immunity**	
Cotl1	coactosin-like 1	1.88	Immunity	
Cuzd1	**CUB and zona pellucida-like domains 1**	**2.84**	**Immunity, auto-immune**	
Defb11	defensin beta 11	1.71	Immunity, innate	
Defb2	**defensin beta 2**	**2.03**	**Immunity, innate**	
Defb42	**defensin beta 42**	**2.47**	**Immunity, innate**	
Defb43	**defensin beta 43**	**2.19**	**Immunity, innate**	
Emb	embigin	1.64	Immunity	
Il4i1	interleukin 4 induced 1	1.71	Immunity, suppressive	
Ly6a	lymphocyte antigen 6 complex, locus A	1.97	Immunity	
Pglyrp1	peptidoglycan recognition protein 1	1.84	Immunity, innate	
Sirpa	signal-regulatory protein alpha	1.64	Immunity	
Plau	**plasminogen activator, urokinase**	**2.30**	**Immunity, Wound healing**	
Apoa1	**apolipoprotein A-I**	**4.38**	**Lipid metabolism, PPAR**	
Apoa2	**apolipoprotein A-II**	**14.07**	**Lipid metabolism, PPAR**	
Apoc3	**apolipoprotein C-III**	**3.88**	**Lipid metabolism, PPAR**	
Apoc1	**apolipoprotein C-I**	**2.18**	**Lipid metabolism, PPAR**	
Apoc4	**apolipoprotein C-IV**	**2.21**	**Lipid metabolism, PPAR**	
Apoe	**apolipoprotein E**	**2.43**	**Lipid metabolism, PPAR**	
Acaa1b	**acetyl-Coenzyme A acyltransferase 1B**	**2.11**	**Lipid metabolism, PPAR**	
Mup1	**major urinary protein 1,** (usually secreted by liver, male sexual attractiveness)	**5.93**	**Lipid metabolism, glucose homeostasis**	
Mup3	**major urinary protein 3,** (usually secreted by liver, male sexual attractiveness)	**4.98**	**Lipid metabolism, glucose homeostasis**	
Mup2	**major urinary protein 2, (usually secreted by liver, male sexual attractiveness)**	**2.08**	**Lipid metabolism, glucose homeostasis**	
Akr1b7	**aldo-keto reductase family 1, member B7**	**2.07**	**Lipid, adiposity**	

Am J Chin Med. Author manuscript; available in PMC 2016 May 19.

	Up-regulated in AGN fed mice >60% (Bold font >2 fold)			**AGN-regulated**
Gene Symbol	**Definition**	**AGN/Control**	**Functional category**	**in NE-Ca**
				Zhang MolCar2014
Ces3	carboxylesterase 3	1.86	Lipid metabolism	
Degs1	degenerative spermatocyte homolog 1 (Drosophila)	1.69	Lipid metabolism, adiposity	
Es1	esterase 1	1.70	Lipid metabolism	
Fads1	**fatty acid desaturase 1**	**2.03**	**Lipid metabolism, synthesis**	
Gde1	glycerophosphodiester phosphodiesterase 1	1.64	Lipid, phospholipid and G-proteins	
Mir16	membrane interacting protein of RGS16	1.78	Lipid, phospholipid and G-proteins	
Ckb	creatine kinase, brain	1.62	Energy metabolism	
Ckm	**creatine kinase, muscle**	**2.07**	**Energy metabolism**	
Ckmt2	creatine kinase, mitochondrial 2	1.67	Energy metabolism	
Hmgcs2	3-hydroxy-3-methylglutaryl-Coenzyme A synthase 2	1.69	Energy metabolism, mitochondria	
Pgam2	**phosphoglycerate mutase 2 *(2,3-diphosphoglycerate synthesis; Hb oxygenation)***	**2.50**	**Energy metabolism, glycolysis diversion**	
Atp2a1	**ATPase, Ca++ transporting, cardiac muscle, fast twitch 1**	**6.52**	**Muscle**	Up50
Atp2a3	ATPase, Ca++ transporting, ubiquitous (Sarcoplasmic/ER Calcium ATPases, SERCA)	1.63	Muscle	
Atp1b3	ATPase, Na+/K+ transporting, beta 3 polypeptide	1.79	Muscle/ion transport	
Cox6a2	**cytochrome c oxidase, subunit VI a, polypeptide 2**	**2.86**	**Muscle/heart, mitochondria ATP**	
Myl1	**myosin, light polypeptide 1**	**6.05**	**Muscle**	Up3
Mylpf	**myosin light chain, phosphorylatable, fast skeletal muscle**	**3.02**	**Muscle**	Up79
Myh8	**myosin, heavy polypeptide 8, skeletal muscle**	**2.90**	**Muscle**	Up30
Myl3	**myosin, light polypeptide 3**	**2.49**	**Muscle**	Up62
Mb	**myoglobin**	**2.15**	**Muscle**	Up34
Myh11	myosin, heavy polypeptide 11	1.65	Muscle	
Mylk	myosin, light polypeptide kinase	1.81	Muscle	
Myom1	myomesin 1	1.69	Muscle	
Tnni2	**troponin I, skeletal, fast 2**	**5.52**	**Muscle**	Up21
Tnnc2	**troponin C2, fast**	**3.07**	**Muscle**	Up20
Tnnt3	**troponin T3, skeletal, fast**	**2.72**	**Muscle**	
Tpm2	**tropomyosin 2, beta**	**2.40**	**Muscle**	Up75

Am J Chin Med. Author manuscript; available in PMC 2016 May 19.

	Up-regulated in AGN fed mice >60% (Bold font >2 fold)			**AGN-regulated**
Gene Symbol	**Definition**	**AGN/Control**	**Functional category**	**in NE-Ca**
				Zhang MolCar2014
Acta1	actin, alpha 1, skeletal muscle	1.81	Muscle	Up5
Acta2	actin, alpha 2, smooth muscle, aorta	1.69	Muscle	
Adssl1	adenylosuccinate synthetase like 1	1.73	Muscle	
Eno3	**enolase 3, beta muscle**	**2.06**	**Muscle**	
Pdlim3	PDZ and LIM domain 3	1.94	Muscle	
Rpl3l	ribosomal protein L3-like	1.84	Muscle specific	
Tcap	**titin-cap**	**2.58**	**Muscle**	
Ttn	titin	1.69	Muscle	
Ttr	**transthyretin**	**4.84**	**Neuroprotection**	Dn74
Pvalb	**parvalbumin**	**3.70**	**Neurogenesis**	
Gldc	glycine decarboxylase	1.74	Neurogenesis	
Inmt	indolethylamine N-methyltransferase	1.82	Neuroprotection, transmitter	
Rhobtb3	Rho-related BTB domain containing 3	1.79	Neuroprotection, vesicular transport	
Scin	scinderin	1.77	Neuroprotection, vesicles	
Serpina1b	**serine (or cysteine) preptidase inhibitor, clade A, member 1b**	**5.85**	**Tumor suppressor, anti-invason**	
Serpina1d	**serine (or cysteine) peptidase inhibitor, clade A, member 1d**	**3.98**	**Tumor suppressor, anti-invason**	
Serpina1c	**serine (or cysteine) peptidase inhibitor, clade A, member 1c**	**3.36**	**Tumor suppressor, anti-invason**	
Serpina1f	**serine (or cysteine) peptidase inhibitor, clade A, member 1f**	**3.26**	**Tumor suppressor, anti-invason**	
Serpine2	serine (or cysteine) peptidase inhibitor, clade E, member 2	1.60	Tumor suppressor, anti-invason	
Spink8	**serine peptidase inhibitor, Kazal type 8**	**2.46**	**Tumor suppressor, anti-invason**	
Spink10	serine peptidase inhibitor, Kazal type 10	1.62	Tumor suppressor, anti-invason	
Spink11	serine peptidase inhibitor, Kazal type 11	1.84	Tumor suppressor, anti-invason	
Ambp	**alpha 1 microglobulin/bikunin (inter-alpha-trypsin inhibitor family)**	**3.20**	**Tumor suppressor, anti-invason**	
Wfdc10	**WAP four-disulfide core domain 10 (protease inhibitor)**	**3.19**	**Tumor suppressor, anti-invason**	
Wfdc15b	**WAP four-disulfide core domain 15B (protease inhibitor)**	**2.48**	**Tumor suppressor, anti-invason**	
Camk2n1	calcium/calmodulin-dependent protein kinase II inhibitor 1	1.69	Tumor suppressor	
Cdh16	cadherin 16	1.63	Tumor suppressor, kidney specific	

	Up-regulated in AGN fed mice >60% (Bold font >2 fold)			AGN-regulated
Gene Symbol	**Definition**	**AGN/Control**	**Functional category**	**in NE-Ca**
				Zhang MolCar2014
Cdo1	cysteine dioxygenase 1, cytosolic *(Taurine production)*	1.83	Tumor suppressor, methylation	
Mat1a	**methionine adenosyltransferase I, alpha *(Methionine-Cysteine metabolism)***	**2.23**	**Tumor suppressor, methylation**	
Elf5	E74-like factor 5	1.96	Tumor suppressor, anti-EMT	
Igfbp7	insulin-like growth factor binding protein 7	1.64	Tumor suppressor	
Lrg1	leucine-rich alpha-2-glycoprotein 1	1.79	Tumor suppressor, anti-EMT	
Samd9l	sterile alpha motif domain containing 9-like, transcript variant 1	1.88	Tumor suppressor, methylation	
Aqp1	aquaporin 1	1.66	Solute/ion transport	
Aqp9	**aquaporin 9**	**2.10**	**Solute/ion transport**	
Clcnkb	chloride channel Kb	1.79	Solute/ion transport	
Fxyd4	**FXYD domain-containing ion transport regulator 4**	**2.98**	**Solute/ion transport**	
Ltf	**lactotransferrin**	**2.36**	**Iron transport**	
Scara3	scavenger receptor class A, member 3	1.85	Solute transport, polyanionic	
Slco1b2	solute carrier organic anion transporter family, member 1b2	1.76	Solute/ion transport	
Slco2a1	**solute carrier organic anion transporter family, member 2a1**	**2.52**	**Solute/ion transport**	
Trf	transferrin	1.97	Iron transport	
Ccnd1	**cyclin D1 *(in prostate epithelium acts as AR transcriptional co-repressor)***	**2.18**	**Prostate AR supressor**	
Clu	**clusterin; testosterone-repressed prostate message-2 gene (TRPM-2)**	**2.24**	**Prostate survival protein**	
Crisp1	cysteine-rich secretory protein 1 (male fertility)	1.67	Prostate function	
Svs2	**seminal vesicle secretory protein 2 (male fertility)**	**2.57**	**Prostate function**	
Qsox1	quiescin Q6 sulfhydryl oxidase 1	1.87	Redox, anti-oxidative	Dn57
Sh3bgrl3	SH3 domain binding glutamic acid-rich protein-like 3	1.71	Redox, cardioprotective	
Mgp	matrix Gla protein	1.83	Vascular health, anti-angiogenesis	
Fga	fibrinogen, alpha polypeptide	1.73	Vascular health, clotting	
Fgg	fibrinogen, gamma polypeptide	1.85	Vascular health, clotting	
Cxcl12	chemokine (C-X-C motif) ligand 12	1.64	Vascular health, maturation	
B3gnt8	UDP-GlcNAc:betaGal beta-1,3-N-acetylglucosaminyltransferase 8	1.74	Oncogene-like, invasion	
Hoxb7	homeo box B7	1.74	Oncogene-like	

Am J Chin Med. Author manuscript; available in PMC 2016 May 19.

	Up-regulated in AGN fed mice >60% (Bold font >2 fold)			AGN-regulated
Gene Symbol	**Definition**	**AGN/Control**	**Functional category**	**in NE-Ca**
				Zhang MolCar2014
Mia1	melanoma inhibitory activity 1	1.75	Oncogene-like, invasion	
Sphk1	sphingosine kinase 1	1.64	Oncogene-like, pro-survival	
Tspan8	**tetraspanin 8**	**2.10**	**Oncogene-like, invasion**	Up65

Am J Chin Med. Author manuscript; available in PMC 2016 May 19.

Table 4

Prostate genes suppressed by 1% AGN feeding in male C57BL/6 mice.

Genes in mouse prostate down-regulated by AGN diet feeding for 6 weeks

	Down-regulated in AGN fed mice >40% (bold font >70%)			**AGN-regulated**
Gene Symbol	**Definition**	**AGN/Control**	**Functional category**	**in NE-Ca**
				Zhang MolCar2014
Nupr1	**nuclear protein 1, p8 or Com1**	**0.29**	**Oncogene-like, invasion**	
Rnu6	U6 small nuclear RNA	0.42	Oncogene-like, miRNA regulation	
Cyp2b10	cytochrome P450, family 2, subfamily b, polypeptide 10 (Cyp2b10), variant 2	0.46	Carcinogen activation	
Frag1	FGF receptor activating protein 1 (Frag1)	0.49	Oncogene-like	
Timp4	tissue inhibitor of metalloproteinase 4	0.52	Oncogene-like, invasion	
Acrbp	proacrosin binding protein	0.53	Oncogene-like, spindle function	
Ceacam1	carcinoembryonic antigen-related cell adhesion molecule 1	0.54	Oncogene-like, prosurvival	
Mat2a	methionine adenosyltransferase II, alpha *(function dinstict of Mat1a tumor suppresor)*	0.54	Oncogene-like, methylation	
Gdpd1	glycerophosphodiester phosphodiesterase domain containing 1	0.55	Oncogene-like, choline metabolism	
Ucp1	uncoupling protein 1 *(mitochondria proton carrier, Brown adipose tissue BAT)*	0.57	Oncogene-like, BAT thermogenesis	
Acaa2	acetyl-Coenzyme A acyltransferase 2 (mitochondrial thiolase)	0.58	Oncogene-like, antiapoptotic, mitochondria	
Gjb2	gap junction protein, beta 2	0.58	Oncogene-like, connexin	
Cldn10	claudin 10	0.58	Oncogene-like, invasion	
Grhl1	grainyhead-like 1	0.58	Oncogene-like, EGFR family	
Copz2	coatomer protein complex, subunit zeta 2	0.59	Oncogene-like, proliferation	
Limk2	LIM motif-containing protein kinase 2	0.59	Oncogene-like, prosurvival	
Mapk13	mitogen-activated protein kinase 13	0.59	Oncogene-like, invasion	
Upk1a	uroplakin 1A	0.60	Oncogene-like, invasion	
Aldh3a1	aldehyde dehydrogenase family 3, subfamily A1	0.60	Oncogene-like, cancer stem cell marker	
Ctnnal1	catenin (cadherin-associated protein), alpha-like 1	0.60	Oncogene-like, Wnt signaling	
Abpb	**androgen binding protein beta**	**0.27**	**Prostate protein**	Up23
Adi1	acireductone dioxygenase 1	0.57	Prostate protein, AR-target, fertility	
Svs3b	seminal vesicle secretory protein 3B	0.57	Prostate protein	
Slc12a2	solute carrier family 12, member 2	0.52	Solute/ion transport	Up60

	Down-regulated in AGN fed mice >40% (bold font >70%)			**AGN-regulated**
Gene Symbol	**Definition**	**AGN/Control**	**Functional category**	**in NE-Ca**
				Zhang MolCar2014
Slc26a4	solute carrier family 26, member 4	0.47	Solute/ion transport	Up71
Slc5a8	solute carrier family 5 (iodide transporter), member 8	0.54	Solute/ion transport	
Lrrc52	leucine rich repeat containing 52	0.58	Solute transport, sperm protein	
Cox8b	cytochrome c oxidase, subunit VIIIb *(Mitochondria, Brown adipose tissue thermogenesis)*	0.58	Energy metabolism, BAT thermogenesis	
Gpr83	G protein-coupled receptor 83	0.37	Energy metabolism, thermogenesis	
Rnf186	ring finger protein 186	0.53	ER-stress apoptosis	
Abo	ABO blood group (transferases A, alpha 1-3-galactosyltransferase)	0.46	Cell adhesion	Up29
Agtr1a	angiotensin II receptor, type 1a	0.55	Vascular health, hypertension	
Azgp1	alpha-2-glycoprotein 1, zinc	0.59	Adipokine, Immunity	Up7
Cbr2	carbonyl reductase 2	0.46	Inflammation, prostaglandin synthesis	Up37
Fbxo32	F-box protein 32	0.60	Tumor suppressor	
Gne	glucosamine (UDP-N-acetyl)-2-epimerase/N-acetylmannosamine kinase	0.59	Muscle health	
Prf1	perforin 1 (*pore forming protein*)	0.53	Immunity, Natrual Killer cells	

Am J Chin Med. Author manuscript; available in PMC 2016 May 19.

Table 5

Normalized organ weight and plasma biochemistry of male CD-1 mice treated with AGN extract by daily *i.p.* injection for 4 weeks. N=6 mice per group. male mice

		Normalized organ weight (mg/g)							
		Body weight g	**Liver**	**Kidney**	**Heart**	**Lung**	**Thymus**	**Spleen**	**Prostate**
Control, vehicle	Mean	37.22	48.27	18.03	5.08	6.40	1.20	3.57	3.00
	SE	1.03	1.62	0.58	0.19	0.35	0.18	0.47	0.15
100mg/kg AGN	Mean	34.98	47.57	15.55	4.85	5.85	1.19	2.43	3.06
	SE	1.04	1.87	0.44	0.14	0.30	0.12	0.22	0.20
200mg/kg AGN	Mean	35.33	48.03	15.52	4.94	6.67	1.09	2.84	2.39
	SE	0.75	0.60	0.61	0.29	0.56	0.07	0.20	0.28
300mg/kg AGN	Mean	33.27	51.92	16.29	5.26	6.62	1.25	2.38	3.06
	SE	0.96	2.32	0.36	0.14	0.30	0.43	0.42	0.39
ANOVA significance		Y	N	Y	N	N	N	N	N

		Plasma biochemistry				
		ALP (U/L)	**AST (U/L)**	**ALT (U/L)**	**BUN (mg/dL)**	**Creatinine (mg/dL)**
Control, vehicle	Mean	55.0	137.7	41.7	31.9	0.20
	SE	4.2	8.0	5.3	3.8	0.01
100mg/kg AGN	Mean	68.3	169.3	31.0	28.9	0.19
	SE	3.7	25.1	2.9	2.0	0.03
200mg/kg AGN	Mean	55.3	161.7	36.7	20.5	0.20
	SE	14.7	6.0	2.8	1.0	0.03
300mg/kg AGN	Mean	60.3	112.3	45.7	26.3	0.21
	SE	6.1	6.7	8.1	0.8	0.01
ANOVA significance		N	N	N	Y	N

Table 6

Normalized organ weight and plasma biochemistry of female CD-1 mice treated with AGN extract by daily *i.p.* injection for 4 weeks. N=6 mice per group.

female mice

			Normalized organ weight (mg/g)					
		Terminal Body weight (g)	**Liver**	**Kidney**	**Heart**	**Lung**	**Thymus**	**Spleen**
Control, Vehicle	Mean	29.52	43.52	13.59	5.39	8.43	2.09	4.01
	SE	0.82	1.20	0.69	0.21	0.95	0.15	0.17
100mg/kg AGN	Mean	27.88	46.22	14.53	5.32	8.54	2.15	3.73
	SE	1.09	2.35	0.69	0.21	0.79	0.29	0.29
200mg/kg AGN	Mean	28.15	49.86	13.30	5.49	8.96	1.58	3.59
	SE	0.63	1.15	0.42	0.23	0.80	0.11	0.16
300mg/kg AGN	Mean	27.55	47.85	12.96	5.41	8.53	1.34	2.88
	SE	0.46	0.90	0.45	0.09	0.43	0.19	0.27
ANOVA significance		N	Y	N	N	N	Y	Y

		Plasma biochemistry				
		ALP (U/L)	**AST (U/L)**	**ALT (U/L)**	**BUN (mg/dL)**	**Creatinine (mg/dL)**
Control, Vehicle	Mean	80.5	119.5	29.5	21.3	0.225
	SE	1.5	2.5	0.5	0.2	0.005
100mg/kg AGN	Mean	112.5	137.5	28.0	27.5	0.205
	SE	27.5	19.5	1.0	6.4	0.005
200mg/kg AGN	Mean	78.0	160.0	28.5	27.5	0.2
	SE	32.0	28.0	1.5	1.5	0.005
300mg/kg AGN	Mean	64.5	182.5	32.0	21.8	0.225
	SE	9.5	7.5	4.0	2.1	0.005
ANOVA significance		N	N	N	N	N